

Article

Automated Acid Rock Drainage Indexing from Drill Core Imagery

Matthew J. Cracknell ^{1,2,*} , Anita Parbhakar-Fox ¹, Laura Jackson ^{1,2} and Ekaterina Savinova ³

¹ Transforming the Mining Value Chain, ARC Industrial Transformation Hub, University of Tasmania, Private Bag 79, Hobart, TAS 7001, Australia; anita.parbhakar@utas.edu.au (A.P.-F.); lauraj0@utas.edu.au (L.J.)

² Centre for Ore Deposit and Exploration Science (CODES), University of Tasmania, Private Bag 79, Hobart, TAS 7001, Australia

³ Corescan Pty Ltd., 1/127 Grandstand Road, Ascot, WA 6104, Australia; katerina.savinova@corescan.com.au

* Correspondence: m.j.cracknell@utas.edu.au; Tel.: +61 3 6226 2481

Received: 28 September 2018; Accepted: 29 November 2018; Published: 4 December 2018

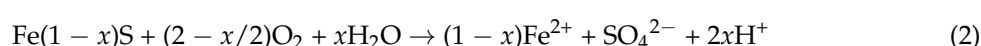
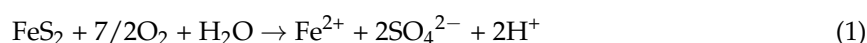


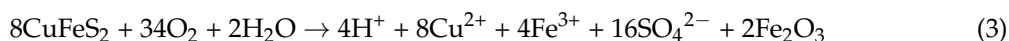
Abstract: The automated classification of acid rock drainage (ARD) potential developed in this study is based on a manual ARD Index (ARDI) logging code. Several components of the ARDI require accurate identification of sulfide minerals that hyperspectral drill core scanning technologies cannot yet report. To overcome this, a new methodology was developed that uses red–green–blue (RGB) true color images generated by Corescan[®] to determine the presence or absence of sulfides using supervised classification. The output images were then recombined with Corescan[®] visible to near infrared-shortwave infrared (VNIR-SWIR) mineral classifications to obtain information that allowed an automated ARDI (A-ARDI) assessment to be performed. To test this, A-ARDI estimations and the resulting acid-forming potential classifications for 22 drill core samples obtained from a porphyry Cu–Au deposit were compared to ARDI classifications made from manual observations and geochemical and mineralogical analyses. Results indicated overall agreement between automated and manual ARD potential classifications and those from geochemical and mineralogical analyses. Major differences between manual and automated ARDI results were a function of differences in estimates of sulfide and neutralizer mineral concentrations, likely due to the subjective nature of manual estimates of mineral content and automated classification image resolution limitations. The automated approach presented here for the classification of ARD potential offers rapid and repeatable outcomes that complement manual and analyses derived classifications. Methods for automated ARD classification from digital drill core data represent a step-change for geoenvironmental management practices in the mining industry.

Keywords: drill core; hyperspectral; prediction; supervised classification

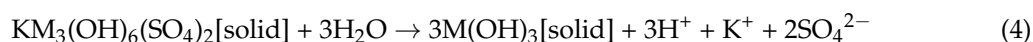
1. Introduction

Accurate classification of the acid forming potential of waste rock is vital to ensure the appropriate management of potential environmental hazards associated with mining operations [1]. One potential hazard is the generation of acid rock drainage (ARD), which forms when iron-sulfide minerals (e.g., pyrite, pyrrhotite, chalcopyrite) contained in mine waste materials (e.g., waste rock, tailings) are exposed to oxygen and water and aided by bacterial catalysis (e.g., *Acidithiobacillus ferrooxidans*, *Acidithiobacillus thiooxidans*, *Leptospirillum ferrooxidans*), undergo oxidation to produce acid, metals and sulfate as shown in Equations (1)–(3) [1,2]:





Whilst other minerals (e.g., sulfates) can also produce acid in a mine waste environment (e.g., Equation (4) where M is Al^{3+} or Fe^{3+} for alunite and jarosite, respectively), the traditional focus in a mine waste characterization program is on iron-sulfides. This is because there is a shorter lag-time to acid generation and they typically dominate the acid forming mineralogy.



Lowering mine drainage pH conditions promotes the mobilization of potentially deleterious metals, which poses severe pollution risks to adjacent and downstream ecosystems with many well documented examples (e.g., Rio Tinto mine, Spain [3–5], Mt. Lyell mine, Australia [6], Iron Mountain mine, United States [7–9]).

Current methods for ARD classification typically follow modifications of the wheel approach [10] or the AMIRA P387A Handbook [11], which focus on the integrated use of static and kinetic chemical tests. These tests involve using small (<10 g) quantities of pulverized representative samples of mine waste to determine their sulfur (or sulfide–sulfur) contents, neutralizing capacity or the amount of acidity generated by oxidation [1,2]. To supplement these labor intensive and subjective assessments of drill core and/or hand specimens, protocols have been developed including the ARD Index (ARDI), which directly calculates the acid-forming (or neutralizing) potential of a rock mass [12]. The ARDI is derived from manual observations of five key indicators of acid-forming potential (A—sulfide content; B—sulfide alteration; C—sulfide morphology; D—primary neutralizer content; and E—sulfide mineral association). ARDI indicator scores are obtained by assessing the concentration, degree of weathering and textural properties (e.g., veined, disseminated or massive) of sulfide minerals, the concentration of neutralizing minerals (e.g., carbonates) and the proximity of chemically reactive or inert minerals to observed sulfides. Each ARDI indicator receives a score from 0 to 10 (except for parameters D and E which are scored from –5 to 10), which are summed together. A maximum of 50/50 (extremely acid forming) and a minimum of –10/50 (potential neutralizing capacity) is permitted. The final ARDI score enables the assignment of a risk ranking; the accuracy of this is enhanced if ARDI values are also screened against total sulfur or paste pH values [12]. However, manual logging methods are often subject to operator bias. Further, manual and analytical approaches are commonly limited by the amount of material (number of samples) that can be assessed due to time and financial constraints.

A key source of information for assessing ARD potential is the estimation of reactive sulfide concentration, typically by using geochemical and mineralogical techniques. For example, sulfide concentrations can be achieved using X-ray diffractometry (XRD), although this is relatively expensive and only possible on a limited number of samples that may not be entirely representative of the rock mass from which they were taken. Other sulfide identification methods use microwave-based infrared (IR) thermography which, in the case of pyrite and chalcopyrite, exploit their semi-conductive properties, which result in more rapid heating than oxides and silicate minerals [13]. However, this is not easily applied to whole drill core and requires imaging to be conducted after heating.

Hyperspectral core scanning platforms such as those provided by Corescan[®], an Australian-based global services company, offer rapid, non-destructive analysis of large volumes of drill core samples using visible to near infrared-shortwave infrared (VNIR-SWIR) data for mineral identification [14]. Such platforms are increasingly being used in geometallurgical characterization programs. However, as sulfides do not have characteristic absorption features in the VNIR-SWIR range of the electromagnetic spectrum, it is difficult to distinguish their presence using these data [15–17]. Bolin and Moon [16] suggested that instead, it may be possible to use red–green–blue (RGB) image data for sulfide identification in conjunction with hyperspectral data in VNIR regions (444–796 nm). In their study, iron-sulfides were identified using supervised image classification. Such an approach would be highly advantageous as it utilizes data that are not only very easy to obtain but is already being collected in a systematic and uniform manner through commercial systems.

In this study, a method for identifying sulfides in Corescan[®] RGB true color imagery was developed and used to calculate A-ARDI values for a suite of drill core materials. The A-ARDI results and classified ARD potential are compared to manually derived equivalents and geochemical- and mineralogical-based classifications as a basis for a discussion on the merits of this approach.

Although this research provides an example of automated mineral identification from RGB and VNIR-SWIR imagery for geoenvironmental applications, the mineralogical information obtained using these methods will also be of benefit to mine-scale spatial and statistical models for geometallurgical applications. For example, accurate estimation of the concentration and spatial context of minerals, including sulfides, identified in drill core collected during resource definition drilling campaigns will benefit strategic planning over the life of the proposed mine by providing information on the spatial distribution of geometallurgically important minerals. Further developments regarding the textural characterization of minerals and mineral assemblages and briefly explored in this research, have implications for optimizing comminution in ore processing systems. The ability to link accurate information on the spatial distribution of minerals and their textural relationships with laboratory and operational data, such as hardness, particle size and alteration characteristics, provide an opportunity to refine, in real-time, metal processing streams to maximize efficiency and recovery.

2. Materials and Methods

Twenty-two core samples collected from one drill hole at a porphyry Cu–Au deposit were used to evaluate A-ARDI classifications. These were specifically chosen as they represent a range of mineralization, texture and alteration characteristics allowing for robust assessment of A-ARDI-based classifications. These samples were imaged by Corescan[®] using the Hyperspectral Core Imager Mark-III (HCI-3) system (Corescan Pty Ltd). The HCI-3 system collects RGB visible wavelength imagery, laser derived digital surface models (DSM), and VNIR-SWIR spectra across the surface of drill core. RGB imagery was collected at a pixel resolution of 60 μm and laser data was collected at a horizontal resolution of 200 μm with a vertical precision of 15 μm . VNIR-SWIR spectra were collected across wavelengths of 448–2500 nm via 514 bands with a spectral resolution of 4 nm and at a spatial resolution of 500 μm . The scanning capabilities and sensor array of the Corescan[®] system allows for rapid, non-destructive imaging of drill core to produce continuous true-color photographs, and VNIR-SWIR derived mineral classifications. Mineral classifications were generated by comparing spectral reflectance signatures to an amalgamated reference spectral library (such as the USGS Spectral Library Version 7 [18]) consisting of more than 1000 separate minerals and mineral sub-species. Through a series of custom algorithms for spectral matching, identified minerals were mapped into visual abundance images and mineral classification maps. The mineral classification maps are a visual display of all interpreted minerals in a single image that captures mineral distributions and relationships, as well as textural variation. Mineral concentrations were obtained by calculating the percentage of pixels classified as a given mineral within a single image.

The input data used to define A-ARDI values were obtained from Corescan[®] RGB true color images, and VNIR-SWIR-based mineral classifications. A-ARDI values were derived using four key stages: (1) identification of iron-sulfide minerals from the supervised classification of RGB image bands; (2) estimation of sulfide and neutralizer mineral (e.g., calcite) concentrations from RGB-derived classifications and VNIR-SWIR mineral classifications, respectively; (3) characterization of sulfide mineral geometries; and (4) quantification of sulfide mineral associations.

To train the sulfide classifier, sulfide and other (all other minerals) class training data were defined by digitizing small regions within representative RGB images. Additional *other* class training data were supplemented by taking a uniform random sample of 5000 pixels within a training image. Classification was carried out on RGB bands and RGB band ratios (R/B, R/G, G/B and $R/B \times G/B$). Training data initially contained an unequal number of sulfide and other class instances. Class imbalance is a significant issue for classifiers that attempt to minimize classification error using 0–1 loss functions [19] such that classifier predictions will be biased towards the majority class. Class imbalance

was addressed by under sampling the majority class (other) by a factor of four using random sampling, and oversampling the minority class (sulfides) via the Synthetic Minority Oversampling Technique (SMOTE; [19]). The resulting balanced training data were combined from 15 drill core samples (some of which were not included in the 22 samples analyzed in this study) to construct a single Random Forests classifier [20].

Random Forests [20] is a machine learning supervised classification algorithm that combines multiple decision trees, based on the Classification and Regression Trees (CART) of Breiman et al. [21], via a majority vote. Individual decision trees are trained using the Gini Index, or similar measure, which identifies optimal splitting thresholds for a given node by maximizing the homogeneity of training samples with respect to candidate classes within the resulting child nodes. Random selection of input features and sampling with replacement (i.e., bagging) ensure that individual decision trees are unique. Class predictions are generated by a vote cast by all decision trees. Class membership probabilities are calculated from the proportion of votes cast for candidate classes across all decision trees [22].

The trained Random Forests classifier was used to predict sulfide or other class labels with associated class membership probabilities for all image pixels (instances) within drill core samples (Figure 1). Sulfide classifications were filtered via a morphological image filter (kernel size 5×5 pixels) that fills in small regions of other classifications within regions classified as dominantly sulfide by growing and then eroding regions of sulfide classifications. The result was further processed using a median image filter (kernel size 5×5 pixels), equivalent to assigning the modal class label within a neighborhood to the center pixel. These image filtering steps smooth sulfide classified images to reduce noise or speckle (Figure 1).

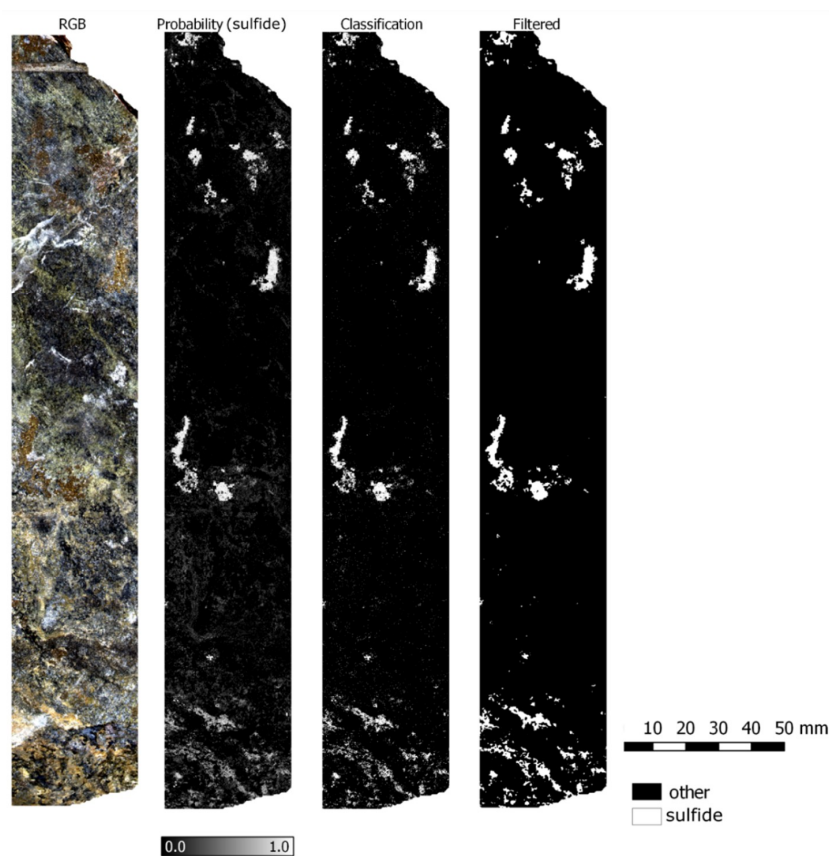


Figure 1. Example of red-green-blue (RGB) image, sulfide class membership probability, sulfide classifications and filtered sulfide classifications for drill core sample 12.

Based on the information in Parbhakar-Fox et al. [12], A-ARDI indicator values were generated by estimating sulfide concentration (e.g., 10% sulfide concentration results in an A-ARDI indicator A value of 1.0) and morphology (i.e., textural characteristics), such as disseminated or massive and degree of veining, from classified images via methods outlined by Cracknell [23]. Carbonate mineral concentrations and sulfide mineral associations were assessed in combination with information from VNIR-SWIR mineral classifications. Indicator values are summed to give the final ARDI value used for acid forming potential classifications (see Table 1 in Parbhakar-Fox et al. [12]). Manually derived ARDI values for the 22 samples following the methodology in Parbhakar-Fox et al. [12] were collected and used for evaluation of and comparison to the A-ARDI classification methodology.

Table 1. Automated and manually derived acid rock drainage (ARD) indicator and index values.

Sample	Manual ARDI						Automated ARDI						Diff. ARDI
	A	B	C	D	E	ARDI	A	B	C	D	E	ARDI	
1	2	10	2	0	0	14	0.5	10	2	0.5	1.5	14.5	0.5
2	1	9	6	-3	-2	11	0	0	0	-3	0	-3	-14
3	1	8	5	-2	-2	10	0	0	0	0	0	0	-10
4	1	8	5	-1	0	13	0	0	0	0	0	0	-13
5	1.5	8	5	-1	-1	12.5	0	0	0	0	0	0	-12.5
6	1.5	10	4	-2	-3	10.5	0	0	0	0	0	0	-10.5
7	3	8	4	-1	-1	13	0	0	0	0	0	0	-13
8	6	9	7	-1	6	27	1	10	5	0.5	1.5	18	-9
9	7	9	7	-1	6	28	2.5	10	5	2.5	2	22	-6
10	6	7	7	6	8	34	2.5	10	6	2.5	0.5	21.5	-12.5
11	5	7	7	-1	6	24	2	10	5	1	2	20	-4
12	2	8	6	-2	3	17	0.5	10	5	0.5	2.5	18.5	1.5
13	1.5	9	8	-3	0	15.5	1	10	5	0.5	0.5	17	1.5
14	1	6	8	1	1	17	0	0	0	0	0	0	-17
15	1	8	7	-1	1	16	0	0	0	0	0	0	-16
16	1	6	5	-2	-1	9	0	0	0	0	0	0	-9
17	2	7	8	-2	0	15	0	0	0	-0.5	0	-0.5	-15.5
18	6	8	8	-1	7	28	2	10	5	2	0	19	-9
19	2	8	9	-2	-1	16	0.5	10	5	0.5	-1.5	14.5	-1.5
20	1	8	7	-1	0	15	0	0	0	0	0	0	-15
21	0	0	0	0	0	0	0	0	0	0	0	0	0
22	1	7	8	-1	1	16	0.5	10	8	0.5	2.5	21.5	5.5

As a further validation measure for both manual ARDI and A-ARDI classifications, mineralogical and geochemical analyses were performed. Mineralogical assessments involved analyses using a Bruker D2 phaser X-ray diffractometer (XRD) (Bruker, Billerica, MA, USA) fitted with a cobalt-X-ray tube at the University of Tasmania (UTAS). Each sample was micronized to 10 μm and loaded into the sample chamber (operating parameters: 30 kV, 10 mA, scan range: 5 to 90° (2 θ), 0.02° step size, 0.6 s per step). Mineral phases were identified using Bruker DIFFRAC.EVA software (version 2.0) package with the PDF-2 (2012 release) mineral database. Semi-quantitative modal mineralogy was calculated using Bruker's proprietary software, Topas (Version 4.2), which enables users to perform Rietveld refinements. Limits of detection ranged from 0.5 to 1.0 wt. % modal abundance. Total carbonate and sulfide values were screened against each other to derive a mineralogical ARD classification [24]. Geochemical static testing included: total carbon (%) and sulfur (%) analyses performed using a Thermo Finnigan EA 1112 Series Flash Elemental Analyser at the Central Science Laboratory, UTAS and Sobek testing, paste pH testing and multi-addition NAG pH testing [25,26] performed at the Earth Science Laboratories, UTAS. Total sulfur values allowed the calculation of maximum potential acidity (MPA, kg H₂SO₄/t) with acid neutralizing capacity (ANC, kg H₂SO₄/t) values derived from Sobek testing [1]. Together these values were used to calculate the net acid producing potential (NAPP = MPA - ANC, kg H₂SO₄/t) which is typically screened against net acid generation (NAG) pH values to give a geochemical ARD classification. As an extra measure, NAG pH and paste pH values were compared to indicate the lag-time to ARD classification [27].

3. Results

Table 1 compares individual A-ARDI indicator values and overall A-ARDI values to those generated using manual observations. Sulfide% based A-ARDI indicator A values are consistently lower than manually derived equivalents. The data presented in Figure 2a and Table 2 suggest estimates of sulfide% from manual observations are overestimated (based on XRD analyses) by 10–40% (mean difference 17.1%). In contrast, the majority of Corescan derived estimates of sulfide% are within $\pm 5\%$ (mean difference -1.2%) of XRD sulfide%. Indicator B values for the A-ARDI approach default to 10 given the lack of Fe-oxides in these samples, and are therefore higher than the equivalent manually derived values. A-ARDI indicator C, based on sulfide morphological characteristics, are typically lower than manually derived equivalents due to differences in sulfide% estimates. Neutralizer% A-ARDI indicator D values are generally higher than manually derived values. Figure 2b and Table 2 show that this difference is due to an overestimation of carbonate mineral abundance from manual observations (mean difference 6.3%) and an underestimation of carbonate mineral abundance from the Corescan mineral classifications (mean difference -5.5%). A-ARDI indicator E values are generally lower than manual estimates for samples where sulfide% is deemed to be approaching 0. Table 1 shows that for the samples with $\sim 0\%$ sulfide minerals classified from RGB imagery A-ARDI values are considerably less (in the order of -10) than manually derived ARDI. Conversely, most of the samples where $\sim 0\%$ sulfide minerals have been classified correspond to manual ARDI indicator A values of 1.5 or less, again highlighting an overestimation of sulfide% from manual observations especially for very low concentrations of sulfides. If samples with very low concentrations (or absence) of sulfides are disregarded, the differences between manual and A-ARDI values indicate overall higher A-ARDI estimates.

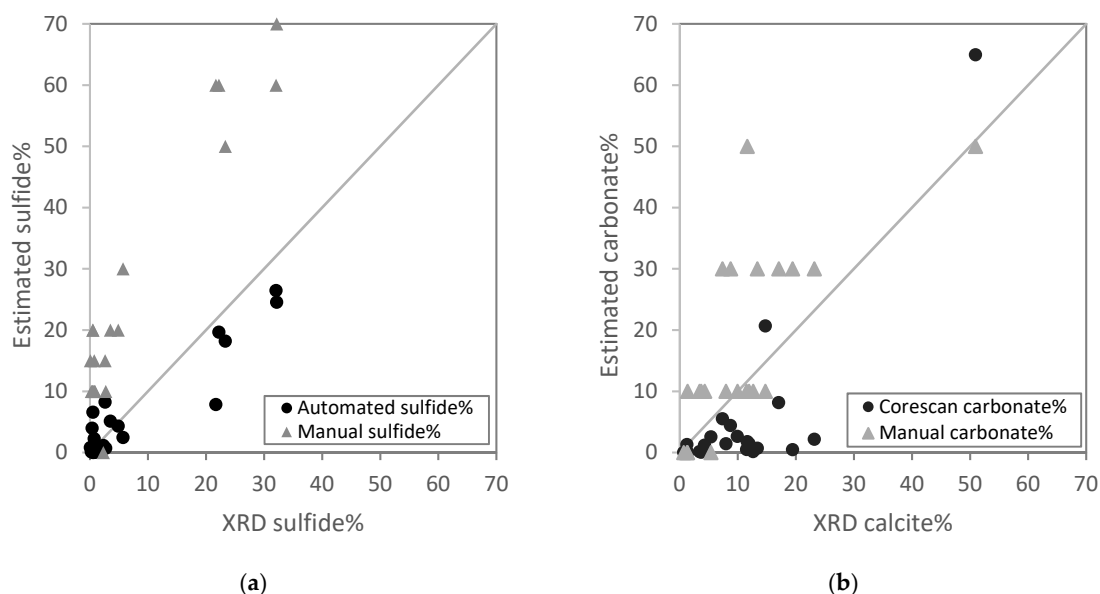


Figure 2. Comparison of XRD derived concentrations and manual and automated estimation of concentration for (a) sulfides and (b) calcite/carbonate minerals. The solid line indicates a 1:1 relationship.

Table 2. XRD derived and automated and manually estimated concentrations of sulfides and calcite/carbonate minerals.

Sample	XRD		Automated/Corescan		Manual	
	Sulfide%	Calcite%	Sulfide%	Carbonate%	Sulfide%	Carbonate%
1	3.5	0.7	5.1	0.0	20	0
2	0.9	50.9	0.0	64.9	10	50
3	2.7	23.2	0.7	2.2	10	30
4	0.3	11.9	0.1	1.5	10	10
5	0.8	11.5	2.3	0.5	15	10
6	0.1	13.4	0.8	0.7	15	30
7	5.7	12.6	2.5	0.2	30	10
8	21.7	8.0	7.9	1.4	60	10
9	32.2	9.9	24.5	2.7	70	10
10	32.1	1.2	26.5	1.3	60	0
11	23.3	14.8	18.2	20.7	50	10
12	4.9	19.4	4.3	0.5	20	30
13	2.6	11.6	8.2	1.8	15	50
14	0.6	1.4	0.0	0.0	10	0
15	0.7	3.7	0.4	0.1	10	10
16	0.4	8.8	0.2	4.4	10	30
17	0.5	17.1	1.0	8.2	20	30
18	22.2	1.3	19.6	0.0	60	10
19	0.5	7.4	6.6	5.5	20	30
20	0.9	4.3	0.1	1.2	10	10
21	2.3	5.4	1.2	2.6	0	0
22	0.4	3.4	4.0	0.2	10	10

Table 3 compares A-ARDI- and manual ARDI-based acid forming potential classifications against those derived using geochemical analyses and XRD-derived mineralogical analyses. Discrepancies between the A-ARDI and NAPP vs. NAG pH classifications are clear. However, the latter is taken to represent a “worst-case” scenario and therefore is forecasting that eventually, if all sulfides are allowed to oxidize with no formation of armoring layers, secondary phases, or alkaline-buffering, a net ARD condition will arise [1]. Automated ARDI comparison against stage-one classifications as per [12] shows further discrepancies for samples 8, 9 and 11. For sample 8, the manual ARDI has identified the ARD potential as PAF (27/50) whilst the A-ARDI classified it as NAF (18/50). ARD classification using XRD values, NAG pH (pH 1.9) and total sulfur (1.35%) also considered this sample as PAF suggesting that the A-ARDI potentially missed a proportion of fine-grained disseminated sulfides, thus assigning a lower score. In the case of sample 9, the manual ARDI score (28/50) is higher compared to the automated value (22/50), however, both classify it as PAF which is likely correct when considering its total sulfur content (4.84%) and NAG pH of 1.8. For sample 11, a lower (by only 4 points) A-ARDI score than via manual observation was obtained. However, geochemical data suggests sample 11 is more likely PAF (total sulfur: 3.72% and NAG pH: 2.2). Again, the automated sulfide classification has encountered difficulties in detecting fine-grained disseminated sulfides due to RGB image resolution limitations while the Corescan[®] mineral classifications have underestimated carbonate% content (Table 2). These drill core materials were unweathered, therefore, high (i.e., >pH 6) paste pH values were obtained and when screened against NAG pH values all samples are, at worst, only PAF with a significant lag-time anticipated for ARD formation [27]. Despite these classification discrepancies, caution must be exercised when using geochemical data only to classify acid forming potential (as extensively discussed in the literature) due to the many limitations associated with individual tests. The supplementation and comparison of these laboratory tests with manual ARDI and A-ARDI outcomes, which include consideration of the textural control on ARD formation, result in an enhanced comprehension of the future waste’s geoenvironmental properties [1,2].

Table 3. Comparison of geochemical, mineralogical and automated ARDI (A-ARDI) classifications (abbreviations: AF, acid forming; ANC, acid neutralizing capacity; NAF, non-acid forming; PNC, potential neutralizing capacity; PAF, potentially acid forming; LR., low risk; UC, uncertain; S, total sulfur).

Sample	GMT Approach: Stage One			GMT Approach: Stage Two				
	ARDI vs. S	S vs. Paste pH	ARDI vs. Paste pH	Paste vs. NAG pH	NAPP vs. NAG pH	XRD	Manual ARDI	A-ARDI
1	NAF	NAF	PNC/NAF	PAF-LR	PAF	NAF	NAF	NAF
2	NAF	NAF	NAF	PAF-LR	UC	NAF	NAF	ANC
3	NAF	NAF	NAF	PAF-LR	NAF	NAF	NAF	PNC
4	NAF	NAF	NAF	PAF-LR	NAF	NAF	NAF	PNC
5	NAF	PAF	NAF	PAF-LR	NAF	NAF	NAF	PNC
6	NAF	NAF	NAF	PAF-LR	UC	NAF	NAF	PNC
7	NAF	NAF	NAF	PAF-LR	UC	NAF	NAF	PNC
8	NAF	NAF	NAF	PAF-LR	PAF	PAF	PAF	NAF
9	NAF	PAF	NAF	PAF-LR	PAF	PAF	PAF	PAF
10	NAF	NAF	NAF	PAF-LR	PAF	PAF	AF	PAF
11	NAF	PAF	NAF	PAF-LR	UC	PAF	PAF	NAF
12	PAF	PAF	PAF	PAF-LR	UC	NAF	NAF	NAF
13	NAF	NAF	NAF	PAF-LR	UC	NAF	NAF	NAF
14	NAF	NAF	NAF	PAF-LR	UC	NAF	NAF	PNC
15	NAF	NAF	NAF	PAF-LR	UC	NAF	NAF	PNC
16	NAF	NAF	ANC	PAF-LR	NAF	NAF	NAF	PNC
17	NAF	NAF	ANC	PAF-LR	UC	NAF	NAF	ANC
18	AF	PAF	AF	PAF-LR	PAF	PAF	PAF	NAF
19	NAF	PAF	NAF	PAF-LR	UC	NAF	NAF	NAF
20	PAF	PAF	PAF	PAF-LR	NAF	NAF	NAF	PNC
21	PAF	PAF	NAF	PAF-LR	UC	NAF	PNC	PNC
22	NAF	NAF	PNC/NAF	PAF-LR	UC	NAF	NAF	PAF

4. Discussion

Despite the fact that sulfides do not display characteristic spectral absorption features at VNIR-SWIR wavelengths [16], Figure 2a and Table 2 show that the discrimination of sulfides from other minerals using RGB true color imagery and Random Forests supervised classification was successful. Nevertheless, Table 2 shows that there is a slight underestimation of automated sulfide% for many samples, which is likely due to RGB image resolution limitations that hinder the discrimination of fine-grained disseminated sulfides. This issue is further compounded by the image filtering steps employed to generate the final sulfide classification. Image filtering, used to reduce false positive classifications resulting from the low spectral resolution of the input features (e.g., RGB bands and associated band ratios), also leads to an increase in size of the smallest sulfide mineral grains that can be identified. Improvements in the detection of fine-grained minerals can only be realized by increasing the resolution of scanners, which Corescan[®] is currently developing, and by careful optimization of image filtering parameters (e.g., kernel size).

On average, the absolute difference between calculated A-ARDI values and manually obtained values is 9. The most obvious discrepancy between manual and A-ARDI classifications arise from contrasting mineral concentration estimates. Across all drill core samples, the calculated sulfide% is up to 40% less than the manual estimate of sulfide% (Figure 2a and Table 2). This difference affects indicator A (sulfide%), indicator C (sulfide morphology) and indicator D (neutralizer%) calculations. Samples with the greatest difference in A-ARDI and manual observations were those which obtained automated sulfide concentrations close to zero. The results presented in Table 2 indicate that the automated sulfide classification of samples with low XRD sulfide% (e.g., <5%) generates approximately equivalent sulfide concentrations. However, the choice of rounding sulfide% to the nearest 5% when calculating A-ARDI indicator A values resulted in many of these samples being assigned a score of 0 (e.g., sulfide% <2.5% generates A-ARDI indicator A values of 0). A potential solution would be to convert sulfide concentrations >1% to an A-ARDI indicator A value of 0.5. This would ensure that only samples with extremely low sulfide concentrations generate an overall A-ARDI value of 0.

Another major discrepancy was the overestimation of parameters D and E when manually assessed (e.g., sample 10). The key contrasts between the results of the automated and manual methods for sample 10 were observed for indicator D (neutralizer%) and indicator E (mineral association) values, which can be attributed to a significant difference in the visual estimation of the amount of carbonate minerals present (Figure 2b and Table 2), with mineralogical classifications showing that the A-ARDI is most likely more accurate.

There were no Fe-oxides identified in the samples assessed and the degree of fracturing has not been estimated. As a result, a default value of 10 was assigned to ARDI indicator B (sulfide alteration). Fe-oxides can be easily identified from VNIR-SWIR hyperspectral data due to characteristic absorption features at near infrared (NIR) wavelengths. However, quantifying degree of fracturing will require alternative information derived from the DSM of the drill core surface. It is therefore reasonable to include parameters representing Fe-oxide content and degree of fracturing into future versions of the A-ARDI.

Whilst the manual ARDI represents the front line in assessing ARD potential in drill core, and should continue to do so with an awareness of its subjective limitations, complementary datasets collected by drill core scanning technologies should be used to assess and validate ARDI results. This will improve deposit-wide characterization for comparison with mineralogical datasets, which provide accurate quantification of the reactive acid-forming and primary neutralizing phases [28], and will show strong classification agreement between both datasets (e.g., ARDI contributing to the refinement of NAF classifications); hence, indicating its robust nature for geoenvironmental domaining. Ultimately, it should be used to complement other geoenvironmental domaining indexes developed specifically for drill core analyses to improve early environmental forecasting and contribute to improve mine-planning activities.

5. Conclusions

This study highlights that rapid and repeatable automated classifications of ARD potential are possible from routinely collected digital drill core data, therefore, maximizing the value of data collecting during early life-of-mine stages. Further, by obtaining this forecasting information, reliable guidance is given for selecting samples for traditional waste classification sampling campaigns. Nevertheless, the automated approach to classification of ARD potential documented here should still be used in conjunction with manual observations and those obtained from geochemical and mineralogical analyses.

A key outcome of this research is the successful automated classification of sulfides from red-green-blue true color drill core imagery. Our results indicate estimations of sulfide percentage concentration from Random Forests classified images is more accurate (mean difference -1.2%) than the manual estimate of sulfide concentration (mean difference 17.1%) when compared to XRD analyses. These observations highlight the challenges faced by human operators in accurately estimating mineral percentages, especially at very low concentrations.

As core scanning technology evolves, higher resolution images and additional data will become available to improve automated sulfide recognition and lead to better geoenvironmental modelling including the classification of acid forming potential, particularly when used in conjunction with other core scanning derived algorithms. Collectively, these tools represent an opportunity to integrate innovative approaches based on emerging technologies and machine learning into ore body characterization for improved environmental planning. This will enable this sector of the industry to move towards its next step-change, whereby static testing, which is fraught with limitations may eventually be superseded by these growing technological capabilities.

Author Contributions: Conceptualization, M.J.C., A.P.-F. and L.J.; Methodology, A.P.-F. and M.J.C.; Software, M.J.C.; Validation, M.J.C., A.P.-F., L.J. and E.S.; Formal Analysis, M.J.C., A.P.-F. and L.J.; Data Curation, L.J. and E.S.; Writing-Original Draft Preparation, M.J.C.; Writing-Review & Editing, M.J.C., A.P.-F., L.J. and E.S.; Supervision, A.P.-F. and M.J.C.; Project Administration, A.P.-F.; Funding Acquisition, A.P.-F.

Funding: This research was funded by Australian Research Council's Industrial Research Hub for Transforming the Mining Value Chain (project number IH130200004).

Acknowledgments: Acknowledgments go to all TMVC and Corescan members for their contributions to this work. We acknowledge the constructive comments from two reviewers that have improved the content of this manuscript.

Conflicts of Interest: The funders had no role in the design of the study; in the collection, analyses, or interpretation of data; in the writing of the manuscript, and in the decision to publish the results.

References

1. Dold, B. Acid rock drainage prediction: A critical review. *J. Geochem. Explor.* **2017**, *172*, 120–132. [[CrossRef](#)]
2. Parbhakar-Fox, A.; Lottermoser, B.G. A critical review of acid rock drainage prediction methods and practices. *SI Process Mineral.* **2015**, *82*, 107–124. [[CrossRef](#)]
3. Hudson-Edwards, K.A.; Schell, C.; Macklin, M.G. Mineralogy and geochemistry of alluvium contaminated by metal mining in the Rio Tinto area, southwest Spain. *Appl. Geochem.* **1999**, *14*, 1015–1030. [[CrossRef](#)]
4. Romero, A.; Gonzalez, I.; Galan, E. Estimation of potential pollution of waste mining dumps at Peña del Hierro (Pyrite Belt, SW Spain) as a base for future mitigation actions. *Appl. Geochem.* **2006**, *21*, 1093–1108. [[CrossRef](#)]
5. Sánchez-España, J.; López-Pamo, E.; Pastor, E.S.; Ercilla, M.D. The acidic mine pit lakes of the Iberian Pyrite Belt: An approach to their physical limnology and hydrogeochemistry. *Appl. Geochem.* **2008**, *23*, 1260–1287. [[CrossRef](#)]
6. Augustinus, P.; Barton, C.E.; Zawadzki, A.; Harle, K. Lithological and geochemical record of mining-induced changes in sediments from Macquarie Harbour, southwest Tasmania, Australia. *Environ. Earth Sci.* **2010**, *61*, 625–639. [[CrossRef](#)]
7. Jamieson, H.E.; Robinson, C.; Alpers, C.N.; Nordstrom, D.K.; Poustovetov, A.; Lowers, H.A. The composition of coexisting jarosite-group minerals and water from the Richmond mine, Iron Mountain, California. *Can. Mineral.* **2005**, *43*, 1225–1242. [[CrossRef](#)]
8. Nordstrom, D.K.; Alpers, C.N. Negative pH, efflorescent mineralogy, and consequences for environmental restoration at the Iron Mountain Superfund site, California. *Proc. Natl. Acad. Sci. USA* **1999**, *96*, 3455. [[CrossRef](#)] [[PubMed](#)]
9. Nordstrom, D.K.; Alpers, C.N.; Ptacek, C.J.; Blowes, D.W. Negative pH and extremely acidic mine waters from Iron Mountain, California. *Environ. Sci. Technol.* **2000**, *34*, 254–258. [[CrossRef](#)]
10. Morin, K.A.; Hutt, N.M. Kinetic test and risk assessment for ARD. In Proceedings of the Fifth Annual British Columbia Metal Leaching and ARD Workshop, Vancouver, BC, Canada, 9–10 December 1998.
11. Smart, R.; Skinner, W.M.; Levay, G.; Gerson, A.R.; Thomas, J.E.; Sobieraj, H.; Schumann, R.; Weisener, C.; Weber, P.A.; Miller, S.D.; et al. *ARD Test Handbook: Project P387, A prediction and Kinetic Control of Acid Mine Drainage*; AMIRA, International Ltd., Ian Wark Research Institute: Melbourne, Australia, 2002.
12. Parbhakar-Fox, A.K.; Edraki, M.; Walters, S.; Bradshaw, D. Development of a textural index for the prediction of acid rock drainage. *Spec. Issue Process Mineral.* **2011**, *24*, 1277–1287. [[CrossRef](#)]
13. Van Weert, G.; Kondos, P.; Wang, O. Microwave heating of sulphide minerals as a function of their size and spatial distribution. *Can. Inst. Min. J.* **2011**, *2*.
14. Schodlok, M.C.; Whitbourn, L.B.; Huntington, J.F.; Mason, P.; Green, A.A.; Berman, B.; Coward, D.; Connor, P.; Wright, W.; Jolivet, J.; et al. HyLogger-3—A visible to shortwave and thermal infrared reflectance spectrometer system for drill core logging—Functional description. *Aust. J. Earth Sci.* **2016**, *63*, 929–940.
15. Clark, R.N.; Swayze, G.A.; Gallagher, A.J.; King, T.V.V.; Calvin, W.M. *The U. S. Geological Survey, Digital Spectral Library: Version 1: 0.2 to 3.0 Microns*; US Geological Survey: Reston, VA, USA, 1993.
16. Bolin, B.; Moon, T. Sulfide detection in drill core from the Stillwater Complex using visible/near-infrared imaging spectroscopy. *Geophysics* **2003**, *68*, 1561–1568. [[CrossRef](#)]
17. Merrill, J.; Martínez, P.; Urrutia, N.; Voisin, L. Sulphides detection by hyperspectral analysis in the thermal infrared range. In Proceedings of the 3rd International Seminars on Geometallurgy (GEOMET), Lima, Peru, 11–13 December 2016.

18. Kokaly, R.F.; Clark, R.N.; Swayze, G.A.; Livo, K.E.; Hoefen, T.M.; Pearson, N.C.; Wise, R.A.; Benzel, W.M.; Lowers, H.A.; Driscoll, R.L.; et al. *USGS Spectral Library Version 7; Data Series*; US Geological Survey: Reston, VA, USA, 2017; p. 68.
19. Chawla, N.V.; Bowyer, K.W.; Hall, L.O.; Kegelmeyer, W.P. SMOTE: Synthetic Minority Over-sampling Technique. *J. Artif. Intell. Res.* **2002**, *16*, 321–357. [[CrossRef](#)]
20. Breiman, L. Random Forests. *Mach. Learn.* **2001**, *45*, 5–32. [[CrossRef](#)]
21. Breiman, L.; Friedman, J.H.; Olshen, R.A.; Stone, C.J. *Classification and Regression Trees*; The Wadsworths & Brooks/Cole Statistics/Probability Series; Wadsworths & Brooks/Cole Advanced Books & Software: Pacific Grove, CA, USA, 1984; ISBN 0-534-98053-8.
22. Hastie, T.; Tibshirani, R.; Friedman, J.H. *The Elements of Statistical Learning: Data Mining, Inference and Prediction*, 2nd ed.; Springer Series in Statistics; Springer: New York, NY, USA, 2009.
23. Cracknell, M.J. Image Texture Quantification from Corescan Mineral Classifications. In Proceedings of the International Association for Mathematical Geosciences, Perth, Australia, 2–9 September 2017; Volume 1, p. 1.
24. Paktunc, A.D. Mineralogical constraints on the determination of neutralising potential and prediction of acid mine drainage. *Environ. Geol.* **1999**, *39*, 103–112. [[CrossRef](#)]
25. Smart, J.; Grimes, K.G.; Douth, H.F.; Pinchin, J. *The Mesozoic Carpentaria Basin and the Cainozoic Karumba Basin, North Queensland*; Department of National Development & Energy, Bureau of Mineral Resources, Geology and Geophysics: Canberra, Australia, 1972; p. 73.
26. Noble, T.L.; Lottermoser, B.G.; Parbhakar-Fox, A. Evaluation of pH Testing Methods for Sulfidic Mine Waste. *Mine Water Environ.* **2016**, *35*, 318–331. [[CrossRef](#)]
27. Weber, P.A.; Hughes, J.B.; Conner, L.B.; Lindsay, P.; Smart, R. Short-Term Acid Rock Drainage Characteristics Determined by Paste pH and Kinetic NAG Testing: Cypress Prospect, New Zealand. In Proceedings of the 7th International Conference on Acid Rock Drainage (ICARD), Louis Missouri, MO, USA, 26–30 March 2016.
28. Maest, A.S.; Nordstrom, D.K. A geochemical examination of humidity cell tests. *Appl. Geochem.* **2017**, *81*, 109–131. [[CrossRef](#)]



© 2018 by the authors. Licensee MDPI, Basel, Switzerland. This article is an open access article distributed under the terms and conditions of the Creative Commons Attribution (CC BY) license (<http://creativecommons.org/licenses/by/4.0/>).